IEEE Photonics Journal
An IEEE Photonics Society Publication

Open Access

The Analysis of Dual-Junction Tandem Solar Cells Enhanced by Surface Dispensed Quantum Dots

Volume 10, Number 5, September 2018

Shun-Chieh Hsu
Yu-Ming Huang
Yu-Cheng Kao
Hao-Chung Kuo, *Fellow, IEEE*
Ray-Hua Horng, *Fellow, IEEE*
Chien-Chung Lin, *Senior Member, IEEE*

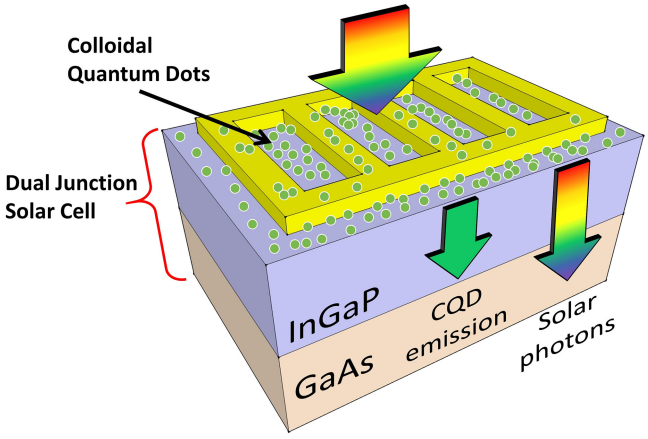

DOI: 10.1109/JPHOT.2018.2865538
1943-0655

IEEE photonics SOCIETY

IEEE

The Analysis of Dual-Junction Tandem Solar Cells Enhanced by Surface Dispensed Quantum Dots

Shun-Chieh Hsu,[1] Yu-Ming Huang,[1] Yu-Cheng Kao,[2] Hao-Chung Kuo,[3] *Fellow, IEEE*, Ray-Hua Horng,[2,4] *Fellow, IEEE*, and Chien-Chung Lin,[1] *Senior Member, IEEE*

[1]Institute of Photonic System, National Chiao-Tung University, Tainan 71150, Taiwan
[2]Graduate Institute of Precision Engineering, National Chung Hsing University, Taichung 40227, Taiwan
[3]Institute of Electro-Optical Engineering, National Chiao Tung University, Hsinchu 30010, Taiwan
[4]Institute of Electronics, National Chiao Tang University, Hsinchu 30010, Taiwan

DOI:10.1109/JPHOT.2018.2865538

Manuscript received June 24, 2018; revised August 5, 2018; accepted August 9, 2018. Date of publication August 14, 2018; date of current version September 11, 2018. This work was supported in part by the Ministry of Science and Technology of Taiwan, ROC, under Grant MOST 104-2628-E-009-013-MY3 and Grant MOST 107-2221-E-009-114-MY3. Corresponding author: Chien-Chung Lin (email: chienchunglin@faculty.nctu.edu.tw).

Abstract: The luminescent down-shifting (LDS) effect of a colloidal quantum dot layer on a dual junction solar cell is explored and analyzed. A 5.47% enhancement of power conversion efficiency is recorded when green quantum dots are dispersed on device surface. The surface reflectance spectra before and after the quantum dot dispenses are necessary to decouple the different mechanisms between antireflective and LDS effects. A further deduction of formulation on the dual-junction device with antireflection and LDS effect is presented and as high as 44.6% of short-circuit current increase in the green quantum dot case can be attributed to the LDS effect according to our calculation.

Index Terms: Dual junction tandem solar cell, quantum dots, solar cells, GaAs, luminescent downshift effect.

1. Introduction

Due to the concerns of global warming effect and energy crises in the past decades, technologies that can harness solar energy have attracted worldwide attention. Among various candidates suited for this purpose, semiconductor-related photovoltaic (PV) technology is one of the most popular ones. In addition to the common choice of silicon, GaAs is crucial in high-concentration PV applications. GaAs is a direct bandgap material that exhibits high absorption over the entire visible portion of the solar spectrum; therefore, GaAs-based solar cells are regarded as a promising technology for high power conversion efficiency (PCE). Recently, Alta Devices Inc. achieved 28.8% PCE with a GaAs single-junction solar cell, setting a new PV efficiency record [1]. Although GaAs solar cells exhibit favorable material properties, their surface Fresnel reflection and surface recombination loss are high. The Fresnel reflection that is attributable to refractive index mismatch can be effectively suppressed if an intermediate layer is inserted between the air and semiconductor. This layer,

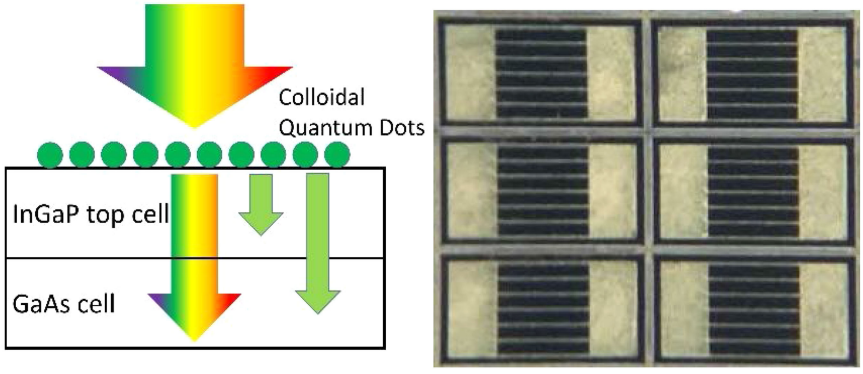

Fig. 1. (a) Schematic diagrams of the dual-junction solar cell with CQDs. (b) Finished devices under optical microscope.

often called antireflective (AR) coating, plays a key role in increasing the photon reception of the device [2]–[4]. In addition to reducing surface reflection, using the full solar spectrum is necessary for further increasing PCE, especially in the ultraviolet (UV) range. High-energy UV photons can be easily absorbed by the material at a shallow depth, but the generated electron-hole pairs are close to the semiconductor surface where recombination loss is high [5]. This problem can be mitigated using certain substances to transform high-energy photons into lower-energy ones; this process is known as luminescent downshifting (LDS) effect [6]–[9]. The LDS effect provides enhancements in the short wavelength response of PV devices by absorbing the UV photons and re-emitting visible ones, which can then penetrate more deeply into semiconductors, and more electron-hole pairs can be collected because of the fewer nonideal recombination centers in the bulk [5], [10]. Hovel et al. first reported in the 1970s that the LDS effect could enhance solar-cell performance at short wavelengths [11]. Studies have examined the use of organic dyes as downshifters [12]–[16]. The organic dye molecules possess poor photostability and narrow absorption spectrum bands, and thus obtaining high PCE is difficult [6], [12], [14], [17]–[19]. In addition to organic dyes, semiconductor-based quantum dots (QDs) or colloidal quantum dots (CQDs) have emerged as another promising LDS materials in recent years [19]–[24]. These QDs are very tiny, usually in the scale of ten nanometers. The confinement in three-dimensional space of electrons and holes leads to quantum mechanically energy level separation and highly efficient photonic transition can be expected [25]. In the past, many excellent experiments and theoretical works related to QD-enhanced LDS effects for PV devices, have been published [21], [23], [26], [27]. These experiments established the prominent role of the QD-assisted LDS effect for the next generation of PV devices. However, most previous works focused on single-junction solar cells that are simple to fabricate and theorize. Multiple-junction solar cells are more complicated and difficult to predict, and few results are available. In this work, QDs were applied to a dual-junction InGaP/GaAs solar cell, and the enhanced PCE was analyzed through detailed measurements of reflectivity, EQE, and photovoltaic I-V characteristics. The theoretical derivation is attempted to reveal the possible way to optimize this LDS effect.

2. Experiment and Devices

The schematic diagram of the dual-junction solar cell can be shown in Fig. 1(a): the top cell is InGaP based design, whereas the bottom cell is made of GaAs. All the dual-junction solar cells had their epitaxial layer structure grown by a metal-organic chemical vapor deposition system (MOCVD), and the epitaxial layer structure is shown in Table 1. The GaAs/InGaP wafers underwent regular semiconductor processes. For GaAs, we used an NH_4OH/H_2O_2 (1:9) etching solution; then, we used a H_3PO_4/HCl (1:2) solution to selectively etch and stop at the proper layer. For contact, the p-type metal was AuBe/Au (45 nm/100 nm) and the n-type metal was AuGe/Au (45 nm/100 nm). During

TABLE 1
The Epitaxial Structure of the Dual-Junction Solar Cells

Layer	materials	Content	Thickness	doping concentration
0	GaAs n-type [Si]	n++ contact	0.3 μm	7x 10^{18}cm^{-3}
1	InAlP n-type [Si]	window	0.03 μm	2x 10^{18}cm^{-3}
2	InGaP n-type [Si]	Emitter	0.05 μm	2x 10^{18}cm^{-3}
3	InGaP p-type [Zn]	Base	0.55 μm	1.5x 10^{17}cm^{-3}
4	AlInGaP p-type [Zn]	BSF	0.03 μm	2x 10^{18}cm^{-3}
5	GaAs[Si]/[Zn]	Tunnel junction	0.015μm x2	1x 10^{19}cm^{-3}
6	InAlP n-type [Si]	window	0.05 μm	1x 10^{18}cm^{-3}
7	GaAs n-type [Si]	Emitter	0.1 μm	2x 10^{18}cm^{-3}
8	GaAs p-type [Zn]	Base	2.5 μm	1x 10^{17}cm^{-3}
9	InGaP p-type [Zn]	BSF	0.1 μm	2x 10^{18}cm^{-3}
10	GaAs p-type [Zn]	p++ contact	0.3 μm	7x10^{18}cm^{-3}
11	AuBe/Au	Bonding layer	0.2 μm	
12	Ni	Substrate	80 μm	

the process, the original GaAs substrate was removed, and the dual-junction epitaxial layers were transferred (upside down) to an 80 μm Ni substrate. Fig. 1(b) shows the finished devices under the optical microscope. The overall processed wafer piece is 1 cm by 1.5 cm and contains 27 individual cells, and the illuminated area for an individual device is 0.9 mm^2.

After the semiconductor fabrication processes were finished, the devices were ready for casting the QD layer. The QD layer, which provides the major LDS effect, comprises CdS/ZnS or CdSe/ZnS core shell–type nanoparticles. For emission wavelengths (λ_{QD}) shorter than 460 nm, the QDs are made of CdS/ZnS, whereas the CdSe/ZnS structure is applied for longer wavelengths (i.e., $>$520 nm). In our experiment, three wavelengths (450 nm, 520 nm, and 640 nm) of QDs were selected on the basis of our previous results [28], and the corresponding samples are labeled as QD450, QD520, and QD640, respectively. All the QDs were purchased from the UT Dots Company. The sizes of the QDs in this paper are: 2.3 nm(QD450), 3.0 nm(QD520), 5.5 nm(QD640), and the three quantum dots all have quantum yields higher than 50% in solvents by the vendor data sheets. The photoluminescence (PL) and absorption spectra of QD450, QD520, and QD640 are shown in Fig. 2. The QDs were stored in toluene with concentration of 5 mg/ml and the micro-pipette was used to cast the QDs on the surface. Every dispense takes 1 μl (one micro-liter) and the quantity was kept the same for all experiments. In Fig. 2(d), the absorption spectra of the dual-junction InGaP/GaAs solar cell and the single junction GaAs solar cell are shown for the comparison. The absorption percentage can be obtained from 100%-(reflection)-(transmission). The black dashed line indicates the bandgap of the $In_{0.47}Ga_{0.53}P$ material and the extra absorption beyond the GaAs single junction solar cell can be attributed to the InGaP layer.

The devices were then placed under simulated AM1.5G light for photovoltaic J-V response. A power supply (Newport 69920), a 1000-W Class-A solar simulator (Newport 91192A) with a Xenon lamp (Newport 6271A) and an Air Mass 1.5, Global (AM1.5G) illumination filter (Newport

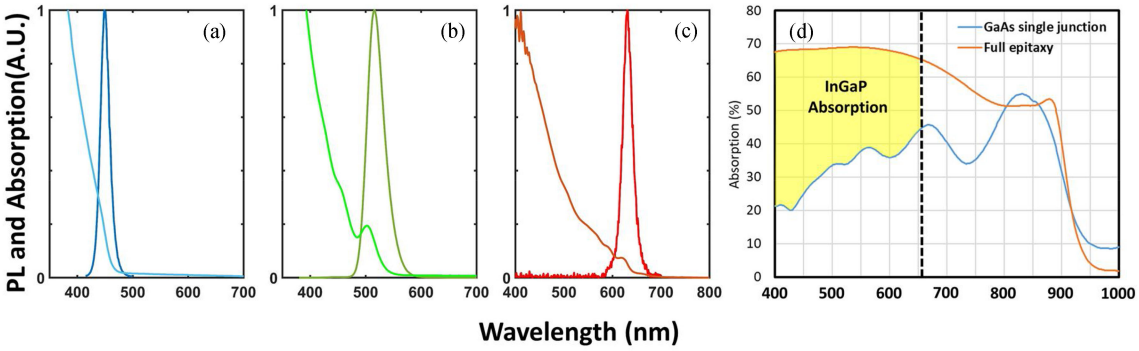

Fig. 2. PL and absorption spectra of (a) QD450, (b) QD520, and (c) QD640. (d) The absorption spectra of the single junction GaAs solar cell (blue) and the full dual-junction InGaP/GaAs solar cell (orange). The dashed black line marks the bandgap of the InGaP material and the yellow region between the blue and orange curves can be viewed as the contribution from the InGaP layer in the device.

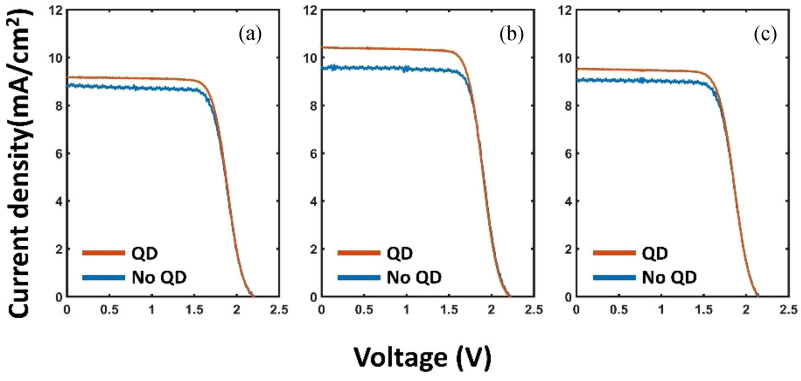

Fig. 3. PV J-V curves of the three samples. (a) QD450 sample. (b) QD520 sample. (c)QD640 sample.

81088A), a probe stage, and a source meter with a 4-wire mode (Keithley 2400) are used for J-V characterization. The accuracy of the measurement is an important factor and it can be estimated by the repeated J_{sc} and V_{oc} acquisition. The stability of probing system and the calibration of the source meters can be carefully monitored and improved by this multiple tests. From the data we obtained, the generic error of the measurement in both J_{sc} and V_{oc} shall be lower than 0.5%. During the enhancement evaluation, the parameters of the same device were used before and after the CQD dispense to eliminate the possible variation among the devices. The external quantum efficiency (EQE) measurement was performed by a system with a Newport 66984 Xenon lamp and a Newport 74112 monchromator [28]. The surface reflection spectra of the device before and after the QD dispense were taken for detailed studies.

3. Measurement Results

Fig. 3 shows the I-V characteristics of the three samples: for the QD450 sample, J_{sc} increases from 8.79 mA/cm^2 to 9.18 mA/cm^2, V_{oc} remains almost the same, and the efficiency rises from 13.78% to 14.3%. For the QD520 sample, J_{sc} increases from 9.53 mA/cm^2 to 10.43 mA/cm^2, and efficiency increases from 15.44% to 16.29%. For the QD640 sample, J_{sc} increases from 9.05 mA/cm^2 to 9.53 mA/cm^2, and efficiency increases from 13.96% to 14.43%. The percentages of J_{sc} enhancement are 4.37%, 9.37%, and 5.35% for the QD450, QD520, and QD640 samples, respectively. The best PCE increment can be seen in QD520 sample, which tops at a 5.47% increase. Table 2 shows the summary of the devices with and without QDs. In Table 3, multiple

TABLE 2
The summarized list of performances of cells with and without QD layers

	QD450		QD520		QD640	
	no QD	with QD	no QD	with QD	no QD	with QD
J_{sc} (mA/cm^2)	8.8	9.18	9.54	10.43	9.05	9.53
V_{oc} (Volt)	2.22	2.2	2.23	2.23	2.15	2.15
Efficiency (%)	13.78	14.3	15.44	16.29	13.96	14.43
Fill Factor	0.7	0.71	0.73	0.7	0.72	0.7

TABLE 3
The standard deviation and average values of J_{sc} and V_{oc} of a generic device with and without QD layers

	J_{sc} (mA/cm^2)	Standard Deviation	V_{oc} (Volt)	Standard Deviation
No QD	8.7590	0.0263	1.9145	0.0007
With QD	10.2598	0.0219	1.9438	0.0042

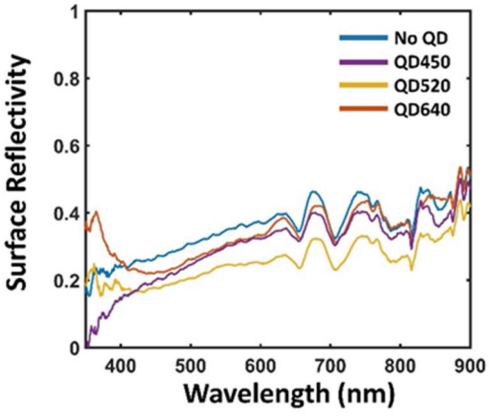

Fig. 4. Reflectivity of the three samples with and without QDs.

measurements were cast to demonstrate the average and standard deviation of a generic cell with and without CQDs.

The overall measurements show that the QD520 sample has a more favorable response in terms of the PCE enhancement. To properly analyze the extent of the LDS effect, the reflectivity and the EQE spectra must be considered as well [27]. Fig. 4 shows the surface reflectivity spectra of the solar cells with and without QDs. All three types of QD samples show reduction of surface reflection due to introduction of the QD layer with an intermediate refractive index. In Fig. 4, the surface reflection of the dispensed devices for different CQDs shows a certain trend at UV wavelength range, i.e., the higher reflection for larger CQDs ($R_{QD640} > R_{QD520} > R_{QD450}$). From the absorption cross-section study in Ref. [29], [30], a larger quantum dot has a much higher absorption cross-section which leads to larger extinction coefficients (n and κ) above the band edge. Because the surface reflection is determined by the difference between the air and the complex refractive index ($n + i\kappa$), it is conceivable that the larger dots can have higher reflective index and thus higher surface reflectivity in the UV range. Fig. 5 shows the EQE spectra from the three samples, and strong enhancement can be found in the green (QD520) sample, whereas the enhancement for the blue QD sample (QD450) and red QD sample (QD640) is not obvious. In general, the strength of the

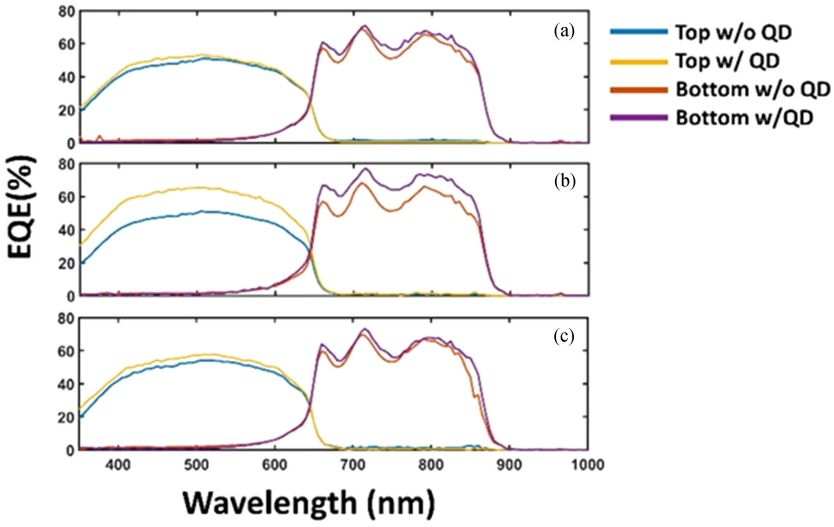

Fig. 5. PV EQE of the three samples. (a) QD450. (b) QD520. (c) QD640.

LDS effect should be evident in the shorter wavelength ranges, particularly beyond the absorption edge in Fig. 2.

Another important parameter that can change the PCE greatly is the fill factor (FF) of the device before and after QD dispense. In some cases, the presence of external materials can be detrimental to the FF due to extra leakage paths created by these add-on particles. In our cases, both J-V curves before and after QD dispense showed very little changes of FF, which indicates our QD layer did not introduce any other current losses.

4. Discussion

This section provides analysis and discussion to specify the operation of the QD-enhanced dual-junction solar cells. In a generic solar cell, when the QD layer is applied to the surface of the solar cells, the surface reflectance was changed due to the additional QD layer with intermediate refractive index, and thus the number of photons received by the device is also changed. At the same time, the QD layer can absorb the UV photons and convert them into visible ones (the aforementioned LDS effect) and provide the solar cell with extra efficiency boost. To accurately estimate the LDS effect, we must consider these changes. On one hand, the photons that enters semiconductors increase because of the anti-reflective property brought by the QD layer, and on the other hand, the down-shifted photons originated from the QDs also impinge upon and get absorbed by the device as well. At longer wavelength range, where the absorption of QD is weak or negligible, only pure AR effect needs to be considered. However, in the shorter wavelength, where the QD absorption is significant, both AR and LDS effects can happen and the situation gets complicated. To properly address this situation, the surface reflection of the device has to be measured to facilitate the analysis. On the basis of our single-junction device results [28], we provide the following formula for short-circuit current density enhancement:

$$\Delta J_{SC} = \int (EQE_{QD} - EQE_{ref}) \times I(\lambda) d\lambda \tag{1}$$

where EQE_{QD} is the EQE of the device with the QD layer, and EQE_{ref} is the EQE without the QD layer and $I(\lambda)$ is the solar spectrum. To further explore, the relationship between IQE and EQE can be used: EQE = IQE$\times$(1-R), and R is the surface reflection of the device [28]. The integral equation

can then be re-arranged into:

$$\begin{aligned}\Delta J_{SC} &= \int \left(\frac{EQE_{QD}}{EQE_{ref}} - 1\right) \times EQE_{ref} \times I(\lambda) d\lambda \\ &= \int \left(\frac{IQE_{QD}(\lambda)}{IQE_{ref}(\lambda)} \frac{(1 - R_{QD}(\lambda))}{(1 - R_{ref}(\lambda))} - 1\right) \times EQE_{ref}(\lambda) \times I(\lambda) d\lambda \\ &= \int [(1 + \Delta_{LDS}(\lambda))(1 + \Delta_{AR}(\lambda)) - 1] \times EQE_{ref}(\lambda) \times I(\lambda) d\lambda \\ &= \int (\Delta_{LDS}(\lambda) + \Delta_{AR}(\lambda) + \Delta_{LDS}(\lambda) \times \Delta_{AR}(\lambda)) \times EQE_{ref}(\lambda) \times I(\lambda) d\lambda \\ &= \Delta J_{LDS} + \Delta J_{AR} + \Delta J_{coupled}, \end{aligned} \tag{2}$$

where IQE_{QD} is the internal quantum efficiency (IQE) of the whole device with the QD layer, IQE_{ref} is the IQE without the QD layer. Notably, two factors are vital in this formula: one is enhancement through the antireflection effect (represented by Δ_{AR}), and the other is enhancement attributed to the LDS effect (represented by Δ_{LDS}).

In equation (2), the term $(1 + \Delta_{LDS})$ is the ratio of IQE values (IQE enhancement), and the $(1 + \Delta_{AR})$ term is the ratio of changed surface reflection (AR enhancement). We believe that the comparison of efficiency enhancement should be based on the same number of received photons; therefore, the effect of surface reflection must be decoupled. By taking out the AR enhancement term, the factor that can increase solar cell's quantum efficiency can only come from the extra down-shifted photons from QDs, and thus the IQE enhancement can be viewed as the LDS related term. The overall enhancement, which can be obtained through EQE measurement, can be written as follows [28]:

$$\text{Overall\_Enhancement} = \frac{EQE_{QD}}{EQE_{ref}} = \frac{EQE_{QD}}{EQE_{NO\_QD}} = (1 + \Delta_{LDS}(\lambda))(1 + \Delta_{AR}(\lambda)) \tag{3}$$

According to this relationship, overlapping EQE enhancement with the AR enhancement profile obtained from the reflection spectrum can reveal whether any LDS effect exists in the device. If the external enhancement is higher than the AR enhancement curve, the value of $(1 + \Delta_{LDS})$ would exceed 1; therefore, Δ_{LDS} would exist. However, if the external enhancement is close to or even lower than the AR enhancement curve, then two possibilities can be referred: either extra scattering loss or absorption in the QD layer such that the LDS effect is suppressed. Generally, a peak (for a favorable LDS effect) or a notch (for strong absorption by QDs) can be found in the UV region, whereas a close match between the AR enhancement curve and EQE ratio profile at long wavelengths can be expected because the effects of LDS are negligible and only the antireflection effect occurs in this longer wavelength range.

In addition to EQE, one can analyze further on the IQE of a photovoltaic device. As stated previously, the IQE response is the part that exclude the surface reflection effect. In a single junction device, the IQE with the QD layer when compared to no-QD case can be formulated as [28]:

$$IQE_{QD}(\lambda) = (1 - A_{QD}(\lambda)) \times IQE_{ref}(\lambda) + \eta_{LDS}(\lambda) \times A_{QD}(\lambda) \times IQE_{ref}(\lambda_{QD}). \tag{4}$$

where A_{QD} is the absorption of the QD layer, η_{LDS} is the photon ratio of emission over the absorption in the QDs, and it can be regarded as the LDS efficiency. The first part of the Eq. (3) describes the efficiency of unabsorbed high energy photons and the second part describes the situation that when certain amount of high energy photons gets absorbed by QDs and re-emiting the visible photons ($\eta_{LDS}(\lambda) \times A_{QD}(\lambda)$ term) at λ_{QD}. With Eq. (1) to Eq. (4), one can calculate the single junction solar cell when the QD layer is presented. When dealing with the incident light and the CQD particles, it is natural to consider the generic theory like Mie scattering to determine the absorption and the reflection/anti-reflection effects. However, the range of wavelengths we are interested covers from 300 nm to 700 nm, and the size of the particles are between 2 to 6 nm. As pointed out previously [29],

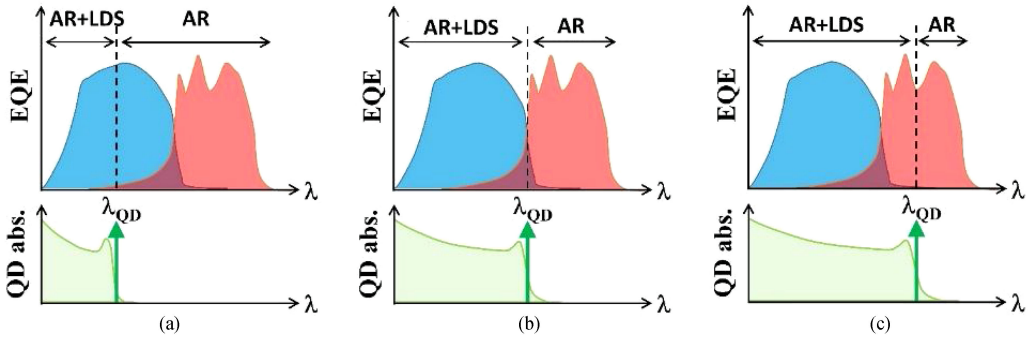

Fig. 6. Three cases for the emission wavelength location of the QD layer: (a) λ_{QD} in the spectral range of the top cell (b) λ_{QD} between the top and bottom cells (c) λ_{QD} in the spectral range of the bottom cell. The bottom plots indicate the corresponding QD emission wavelengths and absorption spectra.

due to this enormous difference in the incident photon wavelength and particle size, the scattering cross-section of the CQD can often be neglected when compared to regular material absorption in the extinction cross-section summation. In the short wavelength region of this study, we tend to model the whole CQD structure as an ensemble and treat it as an emissive and absorptive layer and the negligible scattering loss can be embedded in the η_{LDS} and $A_{QD}(\lambda)$ terms. In the longer wavelength region where the surface reflection is important, it is true that the size and packing density of the quantum dots might affect the anti-reflection of the device. If the packing density is high, the same volume might contain more CQDs than the low density surface, which can lead to higher refractive index and different anti-reflection effect. In our model, the surface reflection is a measured parameter, and we do not calculate theoretically the surface reflection due to the different dot sizes or packing densities. The measured surface reflection can then be applied to extract the internal quantum efficiency (IQE) to complete our evaluation.

For the dual junction devices in our study, two factors are essential when considering J_{SC}: the current matching between the top and bottom cells and the emission wavelength of QDs (λ_{QD}). The short-circuit current density of a tandem solar cell is not the sum but rather the smaller one of the two cells. So it is important to match them and certain simulation will be helpful to have an optimal operation condition. As for the emission wavelength of the QDs, where the λ_{QD} locates can determine the way of LDS affecting the cells. Three different conditions can be summarized as: (A) λ_{QD} in the top cell spectral response; (B) λ_{QD} locates in between the spectral responses of two cells; (C) λ_{QD} in the bottom cell spectral response, as shown in Fig. 6. In the case (A), the formula is the same as the single junction device and only the AR portion in the bottom cell need to be considered. In the case (B) & (C), the situation gets more complicated because both the top and bottom cells can react with QD emitted photons. So the Eq. (4) can now be re-written as:

$$IQE_{top\_QD}(\lambda) = (1 - A_{QD}(\lambda)) \times IQE_{top\_REF}(\lambda) + \eta_{LDS}(\lambda) \times A_{QD}(\lambda) \times IQE_{top\_REF}(\lambda_{QD}). \quad (5)$$

$$IQE_{bot\_QD}(\lambda) = (1 - A_{QD}(\lambda)) \times (1 - IQE_{top\_REF}(\lambda)) \times IQE_{bot\_REF}(\lambda) + \eta_{LDS}(\lambda) \times A_{QD}(\lambda) \times (1 - IQE_{top\_REF}(\lambda_{QD})) \times [1 - A_{top}(\lambda_{QD})] \times IQE_{bot\_REF}(\lambda_{QD}), \quad (6)$$

where the $A_{top}(\lambda_{QD})$ is the percentage of photons at QD emission wavelength that are absorbed by the top cell, and this needs to be considered when the QD photons penetrate through the top cell. The variables, such as IQE_{top_QD} and IQE_{bot_QD}, have similar meanings to their single junction counterparts and represent the IQEs of the top and bottom cells with QD layers, respectively. Other explanations of variables in Eq. (6) can be found in single junction case.

Based on this model, we can evaluate the IQE under the influences of QD layers numerically in dual junction devices. In the following analysis, we will use the measured quantum efficiency spectra as an example to emulate the situations under various LDS efficiencies (η_{LDS}). In case (B), the λ_{QD} sits between the two absorption ranges of the top and bottom cells, and thus both of the cells can absorb the re-emitted photons. The calculation shows that the UV part of the EQE can

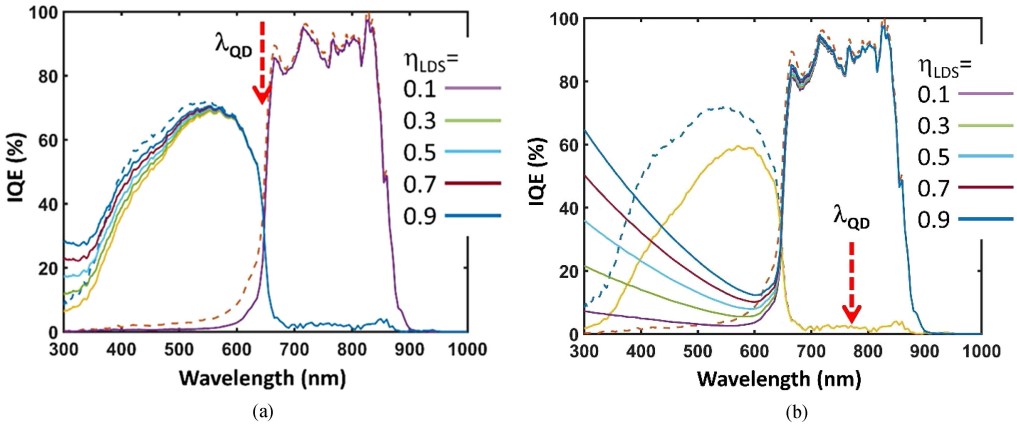

Fig. 7. The dashed EQE spectra are the ones without QDs and obtained from the measurement, blue dash: top cell, red dash: bottom cell. (a) Simulation of IQE with QD layer when the emission wavelength (λ_{QD}) is 640 nm, which is right between the two cells effective absorption ranges. (b) Same calculation but now $\lambda_{QD} = 780$ nm.

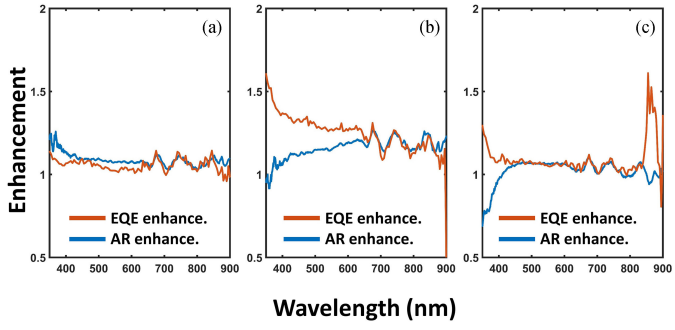

Fig. 8. The EQE and AR enhancement factors of the three samples. (a) QD450. (b) QD520. (c) QD640.

be enhanced as predicted, and the reduction of EQE spectrum in bottom cell at short wavelength region can be attributed to the strong absorption of the QD layer but limited percentage of down-conversion (LDS effect) of photons into electron-hole pairs. For the case (C), the situation is a bit different because now the QD-emitted photons do not get absorbed by the top cell at all. So when a photon with high energ hits the QD layer, the down-shifted photon can penetrate into the bottom cell and produces an electron-hole pair in the bottom cell. The IQE spectral response of the bottom cell is thus enhanced at this short wavelength, as shown in Fig. 7(b). Meanwhile, the top cell EQE is hammered due to the absorption of the QD layer, which does not provide any photovoltaic carriers at all (the QD layer emits photons at λ_{QD} and they are transparent to the top cell). So we can draw a brief summary on the location of the λ_{QD}: if the emission wavelength is too long, it is detrimental to the overall EQE due to the extra absorption in the top cell spectral range and reduction of the quantum efficiency but without the compensation of LDS effect at all. It would be better to put the λ_{QD} in the top cell to substaintiate the LDS effect while using the AR effect in the longer wavelength (the bottom cell) to match the current increment.

Finally, to achieve best enhancement, one must have $\Delta J_{SC\_top} = \Delta J_{SC\_bottom}$. Following the same notation in Eq. (1), both $\Delta_{AR}(\lambda)$ and $\Delta_{LDS}(\lambda)$ are wavelength dependent and the ΔJ_{SC} of the both top and bottom sections need to be equal to maximize the amounts of enhancement (assuming the original J_{SC_top} matches J_{SC_bottom}).

By using the equations from previous sections, one can evaluate the theoretical photovoltaic current based on the reflectance and EQE measurements. Fig. 8 shows both the EQE and AR enhancement spectral responses defined in Eq. (4) from three different QD samples. As been

TABLE 4
The calculated and measured short-circuit current density components in QD-enhanced dual-junction solar cells under different QD emission wavelengths

	QD450		QD520		QD640	
	Top	Bottom	Top	Bottom	Top	Bottom
ΔJ_{sc} (Measured)	0.38		0.89		0.48	
ΔJ_{sc} (Calc.)	1.62	4.33	2.26	1.60	0.45	0.58
ΔJ_{AR} (Calc.)	6.30	6.34	1.12	1.78	0.36	0.28
ΔJ_{LDS} (Calc.)	N/A	0	1.01	0	0.13	0.40
$\Delta J_{coupled}$ (Calc.)	N/A	0	0.13	0	0.02	0

pointed out in previous section, both AR and EQE enhancement factors are close in the long wavelength part of the enhancement factor. Based on the theory developed in previous section, the calculation of J_{AR}, J_{LDS}, and $J_{coupled}$ can be performed, and the results are listed in Table 4. The row of J_{SC}(calc.) was obtained via the measured EQE spectra in Fig. 5 and Eq. (1). While the J_{AR}(calc.) can be calculated from the integration of AR and EQE spectral response, and the term AR can be extracted via the ratio of surface reflectances in Eq. (4). The other terms, J_{LDS} and $J_{coupled}$ can be subsequently determined if J_{AR} is smaller than J_{SC}. Due to the lower J_{SC} in the top cell (from the EQE in Fig. 5), the enhancement of J_{SC} in the top cells can be realized in all three cases from the calculation. In reality, the increment of J_{SC} is actually smaller possibly due to the non-ideal solar simulator spectrum or extra material imperfection. In the case of QD450 device, the anti-reflection effect is so dominating that no LDS enhancement can be expected. In the future, the design rule must be adapted to the asymmetric current distribution. The balance between the enhancement from AR effect and LDS effect and the consideration of no-QD current matching must be taken into account. This rule can be quantified using our experimental data and theory in this paper if the QD layer is deposited under the same condition.

As for the lifetime of such hybrid CQD solar cell, we can evaluate it from two aspects: the LDS phenomenon and anti-reflection effect. For the LDS phenomenon, the luminescent efficiency of the CQD layer needs to be maintained. However, in this study, due to the direct dispense scheme, the dried and unprotected CQD tends to deteriorate significantly (to 35% of its initial value) in five hours according to our previous study [31]. Other methods to seal the CQDs with protective layers are possible, but extra distance of the CQD from the semiconductor surface will create unwanted loss which can in turn degrade the LDS efficiency and need to be carefully balanced. On the other hand, the AR effect brought by the intermediate refractive index of the CQD layer can last much longer because there is no photon-emission involved.

5. Conclusion

In conclusion, we demonstrated the PCE enhancement of a dual-junction solar cell by dispensing CQDs on the device surfaces. The detailed analysis is achieved via reflectance and EQE measurement data. The characterization of LDS effect can be substantiated by considering AR spectral response. For short wavelengths, the enhancement can come from both the photon downshift and AR effects; while for long wavelengths, the AR effect can be dominating. The emission wavelength of CQD is sensitive towards the overall enhancement as we observed green QDs performed better than the other two colors, and this observation complies with our previous report. An extended study can show the numerical model of such devices based on the LDS and AR effects and the importance of the QD emission wavelength (λ_{QD}) in such devices. Further design in terms of current match between multiple junctions is necessary to achieve the full utilization of LDS and AR enhancement. We believe this technology is a great candidate for the next generation of highly efficient PV devices.

References

[1] M. A. Green, K. Emery, Y. Hishikawa, W. Warta, and E. D. Dunlop, "Solar cell efficiency tables (version 41)," *Progr. Photovolt. Res. Appl.*, vol. 21, pp. 1–11, 2013.

[2] M.-A. Tsai, P.-C. Tseng, H.-C. Chen, H.-C. Kuo, and P. Yu, "Enhanced conversion efficiency of a crystalline silicon solar cell with frustum nanorod arrays," *Opt. Exp.*, vol. 19, pp. A28–A34, 2011.

[3] N. Shibata, "Plasma-chemical vapor-deposited silicon oxide/silicon oxynitride double-layer antireflective coating for solar cells," *Japanese J. Appl. Phys.*, vol. 30, 1991, Art. no. 997.

[4] D. J. Aiken, "High performance anti-reflection coatings for broadband multi-junction solar cells," *Sol. Energy Mater. Solar Cells*, vol. 64, pp. 393–404, 2000.

[5] B. Richards, "Luminescent layers for enhanced silicon solar cell performance: Down-conversion," *Sol. Energy Mater. Solar Cells*, vol. 90, pp. 1189–1207, 2006.

[6] E. Klampaftis, D. Ross, K. R. McIntosh, and B. S. Richards, "Enhancing the performance of solar cells via luminescent down-shifting of the incident spectrum: A review," *Sol. Energy Mater. Solar Cells*, vol. 93, pp. 1182–1194, 2009.

[7] B. Richards and K. McIntosh, "Overcoming the poor short wavelength spectral response of CdS/CdTe photovoltaic modules via luminescence down-shifting: Ray-tracing simulations," *Progr. Photovolt. Res. Appl.*, vol. 15, pp. 27–34, 2007.

[8] S. D. Hodgson *et al.*, "Increased conversion efficiency in cadmium telluride photovoltaics by luminescent downshifting with quantum dot/poly (methyl methacrylate) films," *Progr. Photovolt. Res. Appl.*, vol. 23, pp. 150–159, 2015.

[9] B. McKenna and R. C. Evans, "Towards efficient spectral converters through materials design for luminescent solar devices," *Adv. Mater.*, vol. 29, 2017.

[10] X. Huang, S. Han, W. Huang, and X. Liu, "Enhancing solar cell efficiency: The search for luminescent materials as spectral converters," *Chem. Soc. Rev.*, vol. 42, pp. 173–201, 2013.

[11] H. Hovel, R. Hodgson, and J. Woodall, "The effect of fluorescent wavelength shifting on solar cell spectral response," *Sol. Energy Mater.*, vol. 2, pp. 19–29, 1979.

[12] E. Klampaftis and B. Richards, "Improvement in multi-crystalline silicon solar cell efficiency via addition of luminescent material to EVA encapsulation layer," *Progr. Photovolt. Res. Appl.*, vol. 19, pp. 345–351, 2011.

[13] C. Strümpel *et al.*, "Modifying the solar spectrum to enhance silicon solar cell efficiency—An overview of available materials," *Sol. Energy Mater. Sol. Cells*, vol. 91, pp. 238–249, 2007.

[14] B. C. Rowan, L. R. Wilson, and B. S. Richards, "Advanced material concepts for luminescent solar concentrators," *IEEE J. Sel. Topics Quantum Electron.*, vol. 14, no. 5, pp. 1312–1322, Sep./Oct. 2008.

[15] R. Sah, G. Baur, and H. Kelker, "Influence of the solvent matrix on the overlapping of the absorption and emission bands of solute fluorescent dyes," *Appl. Phys.*, vol. 23, pp. 369–372, 1980.

[16] B. Richard and A. Shalav, "The role of polymers in the luminescence conversion of sunlight for enhanced solar cell performance," *Synthetic Metals*, vol. 154, pp. 61–64, 2005.

[17] E. Klampaftis, D. Ross, S. Seyrling, A. N. Tiwari, and B. S. Richards, "Increase in short-wavelength response of encapsulated CIGS devices by doping the encapsulation layer with luminescent material," *Sol. Energy Mater. Sol. Cells*, vol. 101, pp. 62–67, 2012.

[18] D. Ross, E. Klampaftis, J. Fritsche, M. Bauer, and B. S. Richards, "Increased short-circuit current density of production line CdTe mini-module through luminescent down-shifting," *Sol. Energy Mater. Sol. Cells*, vol. 103, pp. 11–16, 2012.

[19] C.-C. Lin *et al.*, "Highly efficient multiple-layer CdS quantum dot sensitized III–V solar cells," *J. Nanosci. Nanotechnol.*, vol. 14, pp. 1051–1063, 2014.

[20] V. Sholin, J. Olson, and S. Carter, "Semiconducting polymers and quantum dots in luminescent solar concentrators for solar energy harvesting," *J. Appl. Phys.*, vol. 101, 2007, Art. no. 123114.

[21] C.-Y. Huang *et al.*, "Efficient light harvesting by photon downconversion and light trapping in hybrid ZnS nanoparticles/Si nanotips solar cells," *ACS Nano*, vol. 4, pp. 5849–5854, 2010.

[22] C.-C. Lin *et al.*, "Highly efficient CdS-quantum-dot-sensitized GaAs solar cells," *Opt. Exp.*, vol. 20, pp. A319–A326, 2012.

[23] F. Purcell-Milton and Y. K. Gun'ko, "Quantum dots for luminescent solar concentrators," *J. Mater. Chem.*, vol. 22, pp. 16687–16697, 2012.

[24] H.-C. Chen *et al.*, "Enhancement of power conversion efficiency in GaAs solar cells with dual-layer quantum dots using flexible PDMS film," *Sol. Energy Mater. Sol. Cells*, vol. 104, pp. 92–96, 2012.

[25] H. Hovel, "The effect of depletion region recombination currents on the efficiencies of Si and GaAs solar cells," in *Proc. 10th Photovolt. Spec. Conf.,* Palo Alto, CA, USA, 1974, pp. 34–39.

[26] A. M. Gabr, A. W. Walker, M. M. Wilkins, R. Kleiman, and K. Hinzer, "Procedure to decouple reflectance and down-shifting effects in luminescent down-shifting enhanced photovoltaics," *Opt. Exp.*, vol. 25, pp. A530–A538, 2017.

[27] S. M. Sze and K. K. Ng, *Physics of Semiconductor Devices*. Hoboken, NJ, USA: Wiley, 2006.

[28] H.-V. Han *et al.*, "A highly efficient hybrid GaAs Solar cell based on colloidal-quantum-dot-sensitization," *Sci. Rep.*, vol. 4, Jul. 18, 2014, Art. no. 5734.

[29] C. A. Leatherdale, W. K. Woo, F. V. Mikulec, and M. G. Bawendi, "On the absorption cross section of CdSe nanocrystal quantum dots," *J. Phys. Chem., B*, vol. 106, pp. 7619–7622, Aug. 1, 2002.

[30] J. Li, J. Chen, Y. Shen, and X. Peng, "Extinction coefficient per CdE (E = Se or S) unit for zinc-blende CdE nanocrystals," *Nano Res.*, vol. 11, pp. 3991–4004, Aug. 1, 2018.

[31] S. C. Hsu *et al.*, "Fabrication of a highly stable white light-emitting diode with multiple-layer colloidal quantum dots," *IEEE J. Sel. Topics Quantum Electron.*, vol. 23, no. 5, Sep./Oct. 2017, Art. no. 2000409.